

Multi-wavelength observations of the Soft Gamma Repeater SGR 1900 + 14 during its April 2001 activation

C. Kouveliotou^{1,2}, A. Tennant², P. M. Woods¹, M. C. Weisskopf², K. Hurley³, R. P. Fender⁴, S.T. Garrington⁵, S. K. Patel¹, and E. Göğüş⁶

chryssa.kouveliotou@msfc.nasa.gov

ABSTRACT

The soft-gamma repeater SGR 1900 + 14 became active on 18 April 2001 after about two years of quiescence; it had remained at a very low state of activity since the fall of 1998, when it exhibited extraordinary flaring. We have observed the source in the gamma and X rays with *Ulysses* and *Chandra*, and in the radio with MERLIN. We report here the confirmation of a two component X-ray spectrum (power law + blackbody), indicating emission from the neutron star surface. We have determined that there is a dust halo surrounding the source that extends up to $\gtrsim 100''$ from the center of SGR 1900 + 14, due to scattering in the interstellar medium.

Subject headings: stars: neutron — stars: magnetic fields

1. Introduction

Soft-gamma repeaters (SGRs) are neutron stars that can be found in a quiescent or in an active state. To date, only four SGRs are confirmed; a fifth SGR source may have been

¹Universities Space Research Association, NSSTC, SD-50, 320 Sparkman Drive, Huntsville, AL 35805, USA

²NASA/Marshall Space Flight Center, NSSTC, SD-50, 320 Sparkman Drive, Huntsville, AL 35805, USA

³University of California, Berkeley, Space Sciences Laboratory, Berkeley, CA 94720-7450, USA

⁴Astronomical Institute “Anton Pannekoek” and Center for High Energy Astrophysics, University of Amsterdam, Kruislaan 403, 1098 SJ Amsterdam, The Netherlands

⁵University of Manchester, Nuffield Radio Astronomy Laboratories, Jodrell bank, Cheshire, SK11 9DL, UK

⁶Department of Physics, University of Alabama in Huntsville, Huntsville, AL 35899, USA

detected twice ((Cline et al. 2000)) but its existence is not yet firmly established. It was recently found ((Kouveliotou et al. 1998; Hurley et al. 1999b)) that SGRs are pulsars with periods ranging within $5 < P < 8$ s, and that these pulsations show rapid spindown of the order of $\sim 10^{-10}$ s/s. As argued by Kouveliotou et al. (1998, 1999) this spindown is due to magnetic dipole radiation (and a relativistic particle wind); the corresponding dipolar component of their magnetic fields exceeds 10^{14} G, thus establishing SGRs as ‘magnetars’, objects initially conjectured in the early 1990s ((Duncan & Thompson 1992; Thompson & Duncan 1995)).

What distinguishes these transient soft γ -ray bursters from the ‘classic’ γ -ray burst sources is the recurrence of their activity and the much softer spectra of their bursts. When active, SGRs emit bunches of up to hundreds of very short, low-energy bursts. The bursts vary in duration and temporal structure from simple, single pulses lasting less than 10 ms, to longer, and more complex events of ~ 100 ms; occasionally highly complex events have been recorded, that comprise over 40 very short subpulses each lasting tens of ms ((Göğüş et al. 2001)).

Very rarely, SGRs emit flares, extremely energetic events (fluences are typically $\sim 10^{44}$ ergs) that are much longer (of the order of several minutes) and exhibit a very hard initial spike (~ 100 ms) and a long soft tail, strongly modulated by the spin of the neutron star. Only two such flares have been detected so far: the 5 March 1979 event from SGR 0526–66 ((Mazets et al. 1979)) and the 27 August 1998 event from SGR 1900 + 14 ((Hurley et al. 1999a; Feroci et al. 2001a)). It is becoming evident, however, that there is a continuum of burst intensities. This is especially clear for SGR 1900 + 14 (where we have the largest sample) but is also observed in SGR 1627–41 ((Mazets et al. 1999; Woods et al. 1999b)). The intermediate size events are roughly 10 – 100 times less energetic than SGR flares, but have a higher energy content ($\sim 10 - 50$ times higher) and are longer than the average SGR burst and relatively uncommon.

We report here on gamma and X-ray observations obtained with *Ulysses*, *Chandra* and on radio observations obtained with MERLIN, soon after the recent reactivation of SGR 1900 + 14, heralded by an intermediate size burst (recorded with the Italian-Dutch satellite *BeppoSAX*) on 18, April 2001 ((Guidorzi et al. 2001a)). Sections 1, 2 and 3 focus on the observations: upper limits in radio wavelengths and spectral and timing results in X-rays. We have searched for evidence of extended emission associated with a dust halo; the source line of sight has a very large N_{H} and such a halo is more or less expected. Our results are discussed in Section 4, where we explore the implications of the current flux level, spectra, timing and halo results for the magnetar model of SGRs.

2. *Ulysses* and MERLIN Observations

On 18 April 2001 *BeppoSAX* was triggered by an intense X-ray burst from SGR 1900 + 14 ((Guidorzi et al. 2001a; Hurley et al. 2001)). The same event was also recorded with *Ulysses*. Triangulation confirmed that its arrival direction was consistent with the position of SGR 1900 + 14. However, the duration and time history of this burst were quite different from typical SGR bursts. The event lasted ~ 40 s, and its time history was modulated with the 5.16 s period of SGR 1900 + 14 ((Hurley et al. 1999b)). Because the *Ulysses* spacecraft was experiencing an intense solar proton flux, the GRB experiment did not trigger on this burst; it was therefore recorded with 0.5 s resolution, and no spectral data are available for it. Nevertheless, we can estimate the peak flux and fluence by assuming that the spectrum may be described by an optically thin thermal bremsstrahlung function with $kT \sim 30$ keV ((Guidorzi et al. 2001b)). The 25 – 100 keV fluence is then $\sim 2.6 \times 10^{-4}$ erg/cm², and the peak flux (integrated over 0.5 s) is $\sim 1.7 \times 10^{-5}$ erg/cm² s. These values are several orders of magnitude greater than those corresponding to the more typical short SGR bursts but roughly 25 and 200 times smaller in fluence and peak flux, respectively, than the giant flare of 27 August 1998 ((Hurley et al. 1999a; Feroci et al. 2001a)). The energetics and the unusual time history of this burst qualify it as an “intermediate event.”

We obtained observations of SGR 1900 + 14 with MERLIN starting ~ 1.6 days after this reactivation. MERLIN is an array of 6 radio telescopes with maximum and minimum baselines of 217 and 10 km connected with 30-MHz bandwidth microwave links to a real-time correlator. SGR 1900 + 14 was observed by MERLIN at 4994 MHz between 23:10 and 11:30 UT on 19/20 April 2001. A 20 arcsec square field was imaged centered on the given co-ordinates of SGR 1900 + 14, with an effective resolution of 75 mas. There were no obvious detected sources in this field. The map co-ordinates are aligned to within ~ 20 mas of the International Celestial Reference Frame via the phase referencing technique. Given the extremely well known location of the source, ((Frail et al 1999)), a reasonable (3σ) upper limit to the 5 GHz radio flux density of SGR 1900 + 14 is 0.45 mJy.

3. *Chandra* Observations

Chandra observed SGR 1900 + 14 on 22 and 30 April, 2001, starting at 04:39:18 UT and 23:09:50 UT, respectively. The two sets of 20 ks observations were both taken with ACIS-S3 in the Continuous Clocking (CC) mode. We detect a single burst of 14 photons in the first data set, which appears to be real. Due to the small number of detected photons, however, we will not discuss the event any further and we will restrict ourselves to pulse timing, spectral and spatial analysis of the persistent source as described below.

3.1. Timing Analysis

In CC mode data, the charge packet generated by a photon is clocked out of the detector at the rate of 2.85 msec per row. Thus for a photon that interacts near the center of a CCD, it will take ~ 4.3 s until the time the charge is read out of the frame store and the timetag is applied. This is further complicated by the spacecraft dither which moves the image on the detector, causing the delay to vary accordingly. We have written a simple ftools script that corrects for this delay. The axBary program is then applied to correct the times to the solar system barycenter.

We have folded the data on the period derived with our *RXTE* observations of 5.17282 s ((Woods et al. 2001b)). We used a spline fit to the data to define a pulse profile. This profile is then cross-correlated with 776 s subsets (i.e., 150 cycles each) of the data and the time offset defines a local measurement of the phase (Figure 1). The upward trend indicates that the best fit period for the *Chandra* data (5.17293(4) s) differs slightly but significantly from the *RXTE* value. The period measurement errors are given in parenthesis and represent the 1σ uncertainty in the least significant digit. For the second *Chandra* observation, we find good agreement between our measurement ($P = 5.17293(5)$ s) and the *RXTE* ephemeris.

We see in Figure 1 that there are systematic deviations suggestive of a sine wave. When we allow for a sine wave in our fitting we obtain an F statistic of 7.0, which for the 3 additional parameters is significant at about the 92% level. We do not feel that these residuals reflect a real orbital period; they are most likely due to phase noise (it is quite possible that the timing noise detected here is responsible for the disagreement between the periods derived with *RXTE* and *Chandra*). However, since the period (5500 sec or about 92 min) would be extremely difficult for a satellite in low Earth orbit to detect, we feel that it is important to set here an upper limit; the 90% confidence upper limit on the period amplitude is 0.25 s.

We compared the pulse profile in different energy bands (0.5–1.7, 1.7–3.0, and 3.0–7.0 keV) to investigate shape-energy dependence. We do not see any significant differences in the pulse shape with energy, within statistics. We find that the 0.5–7 keV rms pulse fraction is 16.2(9), and 14(1)% during the first and second observation, respectively.

3.2. Spectral Analysis

We extracted a six pixel wide spectrum centered at the peak of the source image. Since in the continuous clocking (CC) mode, events anywhere in a CCD column will be read out at the same collapsed CC location, this region maps onto the sky as a rectangle $3''$ high and $8.3'$ long rotated by the spacecraft roll angle. To allow normal χ^2 fitting, we grouped the

spectrum into bins, which contain a minimum of 40 counts each.

We used CIAO (Version 2.1.1) to compute a response matrix assuming a point source at the center of the CCD. It is also worth noting that the CC mode used on-orbit was never calibrated on the ground. Although the on-orbit version of continuous clocking better approximates Time Exposure (TE) mode data and therefore the CIAO computed matrix is a good approximation, minor differences between the data and model should be treated with a good deal of skepticism.

We used XSPEC ((Arnaud 1996)) to fit the spectra. The measured spectral parameters and χ^2 values for all fits are listed in Table 1. For both data sets we find that the spectrum can be fit with an absorbed power law; the corresponding unabsorbed (2 – 10 keV) fluxes are 1.20(3) and $1.00(3) \times 10^{-11}$ ergs/cm² s, for the first and the second observation, respectively. We find that in the second data set the flux decreases by 20% from the first observation, in agreement with what has been reported by (Feroci et al. 2001b), and that the spectral index is slightly steeper (by 0.1).

To optimize the statistics we added the two data sets; Table 1 shows that a single power law model is a poor fit. To improve our fit we (i) ignore channels between 1.8 and 2.5 keV since most of the residuals occur from the Si K line (from the detector) to the Ir edge (from the mirror) and hence are probably instrumental, and (ii) we add a blackbody (BB). The BB addition gives an F statistic of 20.3; the probability that the χ^2 improvement is a chance coincidence is 4×10^{-5} . We find that 19% of the unabsorbed (2 – 10 keV) flux comes from the blackbody component, i.e., $0.21(5) \times 10^{-11}$ erg/cm²s. The best fit parameters are in agreement with our earlier work ((Woods et al. 1999a; Woods et al. 2001a)).

Finally, we took the best fitting blackbody parameters from the summed spectrum and added it to our model for the first and second data sets. We did not allow the BB temperature nor the normalization to vary and refit for the power law parameters and N_H . The PL + BB fit fluxes are identical to their single PL values. Although the errors are relatively large, it is interesting that the entire difference between the two data sets can be modeled with the change of a single model parameter (i.e., the power law normalization).

Figure 2 shows the data of the first *Chandra* observation fit with a two-component (PL + BB) spectral model (solid line). We do not observe any significant features in the spectrum; we have investigated, however, the significance of the small excess at 3.15 keV. The addition of a line in the model for the first data set (at 3.15 keV) decreases the F statistic by 6.7 which is less than 3σ . The significance is further reduced if one considers that the residuals are similar in amplitude to the Ir edge features near 2.1 keV, and that a 2σ deviation is expected somewhere in the spectrum from chance alone. Further the feature is not seen in

the second data set nor in the summed set. Therefore we do not feel that the line is real. However, we can use it to set an upper limit for a line detection. The 90% confidence upper limit on the line rate is 2.0×10^{-5} photons/cm² s, corresponding to an equivalent width of 38 eV.

3.3. Search for extended emission

Given the large column to SGR 1900 + 14 we *expect* a dust scattering halo surrounding this X-ray source. To search for this as well as for the presence of any hypothetical X-ray nebula, we investigated the 1-dimensional CC image. We found no significant point sources other than the SGR; for each pointing we generated two images within the 0.5–7 keV energy band. The first image is simply the time-integrated image. We approximated the internal instrumental and diffuse Galactic plane background on chip S3 by using data from the other back-illuminated CCD S1. We measured the average rate on S1, corrected for the absolute normalization (between 0.5–7 keV) at the same focal plane temperature between the two chips S1 and S3 ((Markevitch & Vikhlinin 2001)), and then subtracted the S1 average (DC) level from chip S3.

Next, we generated a “pulsed” image for each observation. We convolved the event list for S3 with the observed source pulse profile normalized to a mean of zero to generate a background-subtracted image. That is, events recorded near pulse maximum received a positive weight and those during pulse minimum, a negative weight. Applying this technique, we removed all emission components in our image that do not vary in phase (i.e., everything except the pulsar photons).

We compared the time-integrated images and found no significant difference between them. To improve our statistics, we then averaged first the time-integrated images and separately the pulsed images for the two observations and folded the 1-D images about each centroid to accumulate “quasi-radial” profiles (these are not true radial profiles because the CC mode data were first collapsed in one dimension). The time-integrated and pulsed profiles are shown in Figure 3 in addition to a MARX PSF model (dotted line) scaled to the normalization of each. As expected, the pulsed image is entirely consistent with the model PSF. However, due to the small pulse fraction of this source, the pulsed image has a relatively poor signal-to-noise ratio, which is reflected in the rather large error bars. We find a significant excess above the model PSF for the time-integrated image further than 3'' away from the centroid. This excess contributes < 0.5 % to the total flux and can be attributed to a dust halo. We discuss these results in the next section.

4. Discussion

We have observed in the past that SGR activity results in an increase of the persistent X-ray flux; the flux then decays following a power-law function with varying temporal indices for different sources. For SGR 1900 + 14, the ‘nominal’ (baseline) 2–10 keV flux is $\sim 1 \times 10^{-11}$ ergs cm² s⁻¹ and the temporal decay index was found to be 0.6–0.7 during its previous activation in 1998 ((Woods et al. 2001a; Ibrahim et al. 2001)). The recent flaring activity of the source has decayed with a similar index of ~ 0.6 ((Feroci et al. 2001b)). These results seem to indicate an intrinsic luminosity relaxation time constant per SGR source, that appears to be independent of the activity level.

We have shown earlier that the overall increase of the source intensity is entirely due to the power law component of the spectrum ((Woods et al. 1999a)). At the peak of activity, the spectrum is best fit with a single power law model; the thermal component reemerges only when the power-law flux reduces to its ‘nominal’ level. Our *Chandra* results confirm the blackbody component in the spectrum of SGR 1900 + 14, which is the *only* SGR that shows clear evidence of thermal emission from the neutron star surface. With regards to its X-ray spectrum, therefore, SGR 1900 + 14 seems to provide yet another link with the other class of objects identified as magnetars, namely the Anomalous X-Ray Pulsars (AXPs). There are so far 5 (maybe 6) AXPs, sources that are very similar to SGRs, with the main exception that they have never been observed to burst ((Mereghetti 1999)).

The radio flux (3σ) upper limit we derived with MERLIN ~ 1.6 – 2.1 days following this flare is both closer in time and slightly above the earlier reported detection level for SGR 1900 + 14 during its 1998 reactivation. VLA measurements at the same wavelength detected a possible peak in the flux of ~ 0.3 mJy ((Frail et al 1999)) ~ 10 days after the huge flare that released $\sim 10^{44}$ ergs in γ -rays. Frail et al. (1999) estimate the minimum energy release in particles necessary to create the detected synchrotron nebula to be of the order of 7×10^{37} ergs; the intermediate burst that triggered the current activity released 25 times less energy in γ -rays. If we scale the particle energy accordingly, we derive an upper limit of 4×10^{35} ergs for any transient synchrotron nebula associated with this burst. Our observations show that a prompt and relatively high-intensity radio flare immediately following an SGR 1900 + 14 outburst is unlikely. Unfortunately, there are no MERLIN or other radio data available for SGR 1900 + 14 at ~ 10 days after its recent outburst.

The observed profile of the extended emission is consistent with scattering of the X rays on the interstellar medium along the line of sight from the source, given the large value of the observed N_{H} ((Predehl & Schmitt 1995)). This is the first detection of a dust scattering halo around a magnetar; unfortunately, due to the large distance of SGR 1900 + 14, any pulsed component is smeared out in the halo preventing the direct measurement of its distance

using its X-ray scattering halo ((Predehl et al. 2000)).

In conclusion, we have provided a constraining upper limit on the radio flux from a transient synchrotron bubble following the intermediate flare of 18 April 2001. We confirmed the thermal component in the spectrum of SGR 1900 + 14 , and have placed a limit on line features in the X-ray spectrum. Utilizing the sensitivity and resolving power of *Chandra* , we have discovered a dust scattering halo surrounding SGR 1900 + 14 . We expect that our upcoming *Chandra* observation (NRA2) will allow for a more detailed study of this halo.

Acknowledgements: We acknowledge support from the following grants: MX-0101 (C.K.), NAG5-9350 (C.K., P.W. and S.P.), GO0-1018X (S.P.), JPL Contract 958056 (K.H.). We are grateful to Peter Thomasson for rapidly arranging the MERLIN scheduling at a very short notice and to Dr. C. Thompson, Dr. R. Duncan, Dr. P. Predehl and Dr. M.S. Briggs for critical discussions on our results.

REFERENCES

- Arnaud, K. 1996, Astronomical Data Analysis Software and Systems V., A.S.P. Conference Series 101, 17
- Cline, T.L. et al. 2000, ApJ 531, 407
- Duncan, R.C., & Thompson, C. 1992, ApJ, 392, L9
- Feroci, M. et al. 2001a, ApJ, 549, 1021
- Feroci, M. et al. 2001b, GCN #1055
- Frail, D. A. et al. 1999, Nature398, 127
- Göğüş, E. et al. 2001, ApJ in press
- Guidorzi, C. et al. 2001a, GCN #1041
- Guidorzi, C. et al. 2001b, IAU Circ., No. 7611
- Hurley, K. et al. 1999a, Nature, 397, 41
- Hurley, K. et al. 1999b, ApJ, 510, L111
- Hurley, K. et al. 2001, GCN # 1043
- Ibrahim, A. et al. 2001, ApJ in press (astro-ph/0007043)

- Kouveliotou, C. et al. 1998, *Nature*, 393, 235
- Kouveliotou, C. et al. 1999, *ApJ* 510, L115
- Markevitch, M. & Vikhlinin, A. 2001, *Apj* in press, astro-ph/0105093
- Mazets, E.P. et al 1979, *Nature*, 282, 587
- Mazets, E. et al. 1999, *ApJ* 519, L151
- Mereghetti, S. 1999, in *The NS-BH Connection*, astro-ph/9912207
- Predehl, P. & Schmitt, J.H.M.M. 1995, *A&A* 293, 889
- Predehl, P. et al. 2000, *A&A* 357, L25
- Thompson, C. & Duncan, R.C. 1995, *MNRAS*, 275, 255
- Woods, P. et al. 1999a, *ApJ* 518, L103
- Woods, P. et al. 1999b, *ApJ* 519, L139
- Woods, P. et al. 2001a, *ApJ* 552, 748
- Woods, P. et al. 2001b, *GCN #* 1056

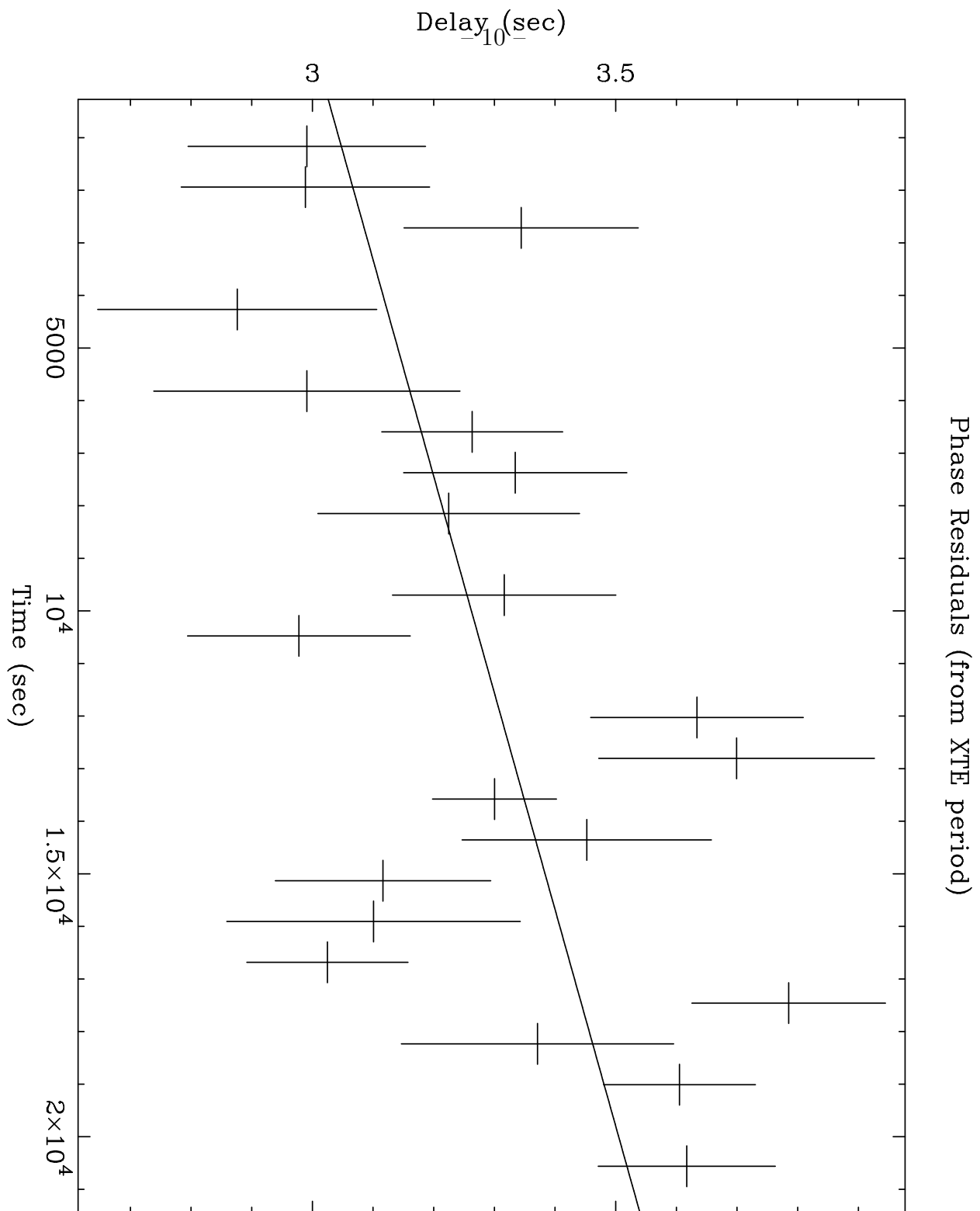


Fig. 1.— The *Chandra* phase residuals (2–10 keV) from the *RXTE* PCA ephemeris for the first observation on April 22. The solid line is a fit to the residuals with a straight line.

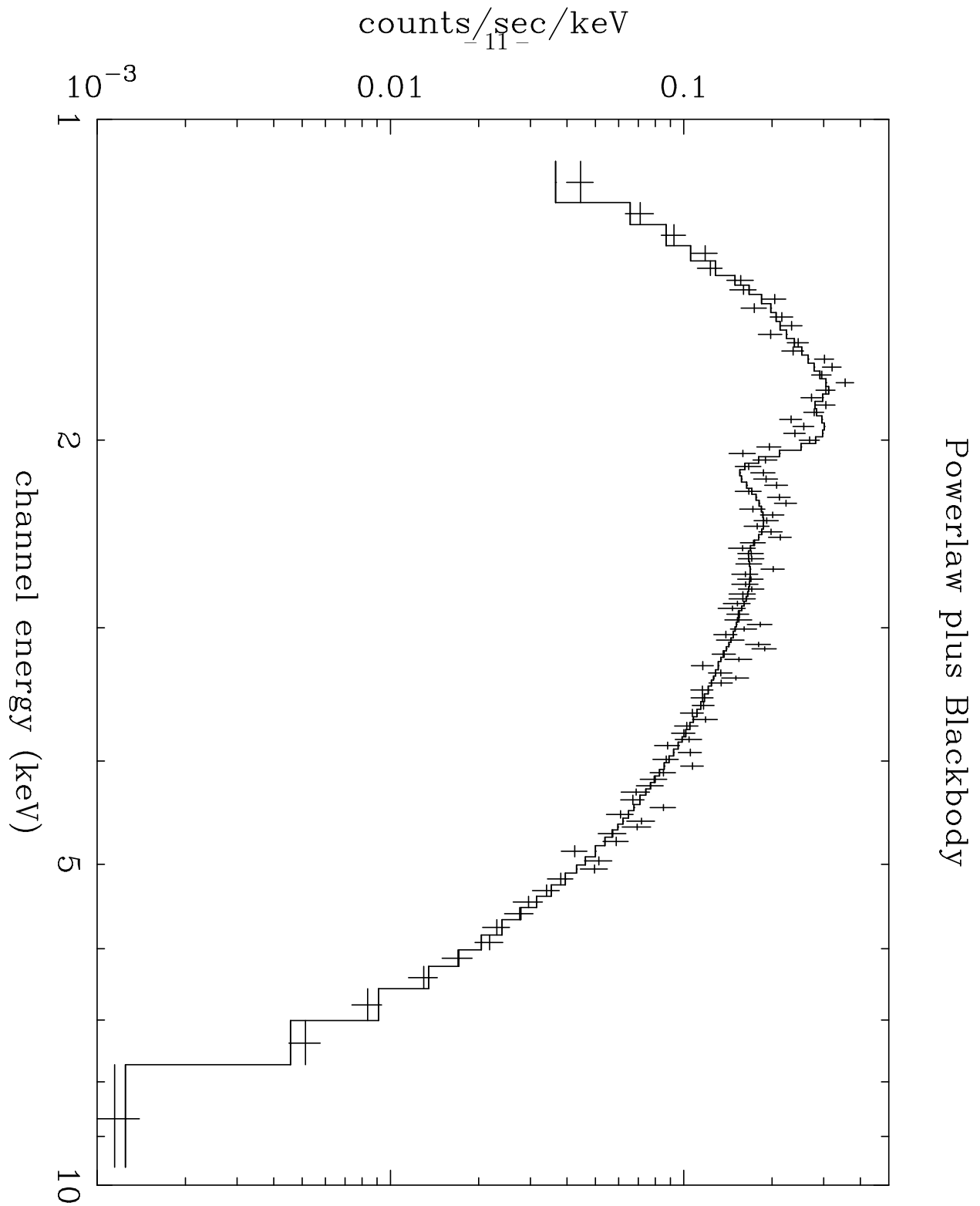


Fig. 2.— The energy spectrum of the first *Chandra* observation of SGR 1900+14 fitted with a power law + blackbody model (solid line).

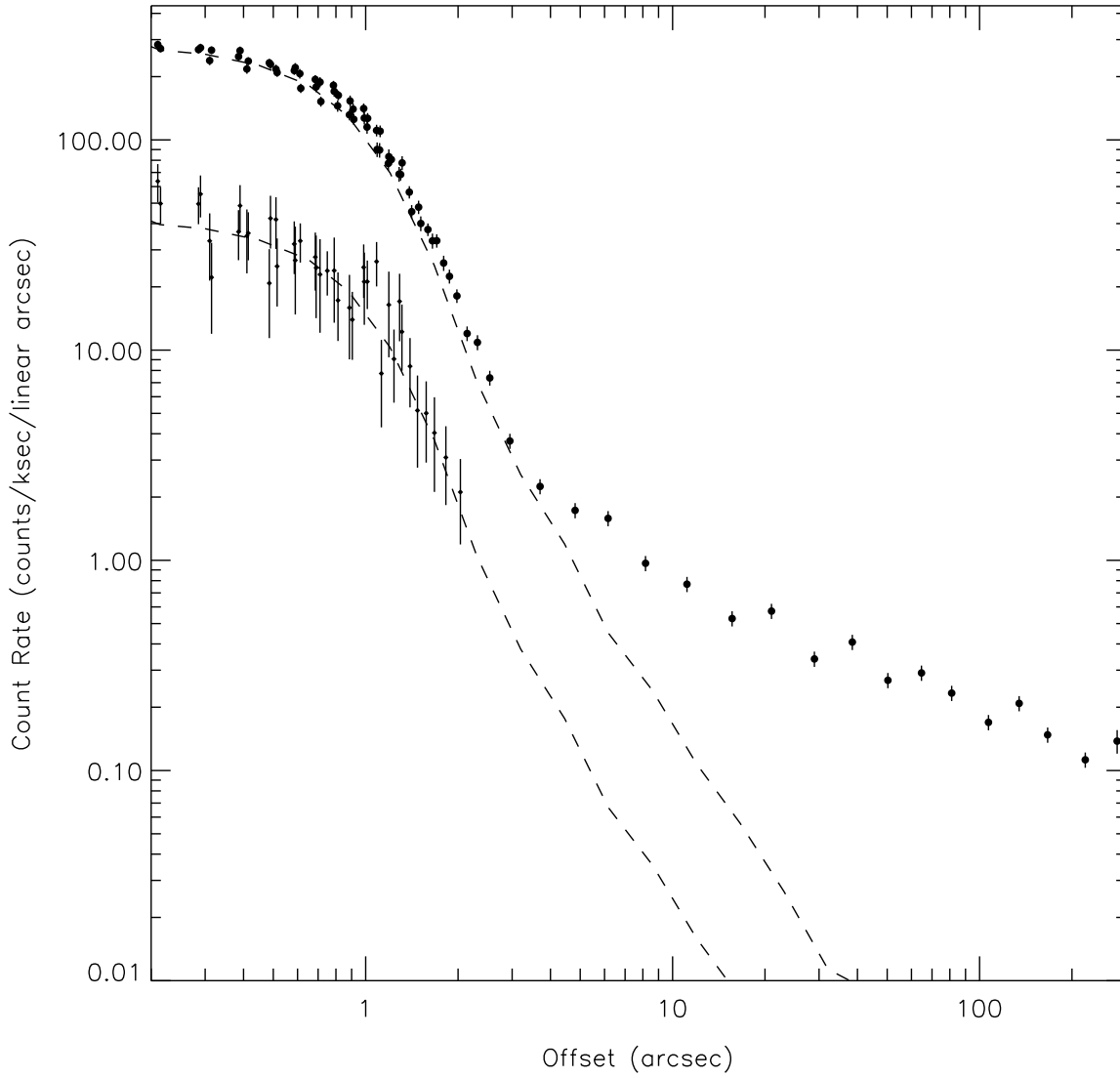


Fig. 3.— The time-integrated (filled circles) and pulsed (diamonds) profiles of SGR 1900 + 14 averaged over both *Chandra* observations. The dotted lines represent the PSF models scaled to the normalization of each profile.

Table 1. Summary of spectral fits.

Date	Model ^a	N_{H} (10^{22} cm^{-2})	Γ	kT (keV)	χ^2/dof
4/22	PL	2.69(10)	2.66(9)	...	232.8/211
4/22	BB+PL	2.44(9)	2.07(10)	0.46	233.3/211
4/30	PL	2.77(12)	2.82(10)	...	210.1/173
4/30	BB+PL	2.40(9)	2.07(13)	0.46	197.8/173
Both	PL	2.73(8)	2.73(7)	...	367.7/272
Both	BB+PL	2.3(2)	2.1(3)	0.50(4)	349.7/279
Both ^b	PL	2.71(8)	2.73(7)	...	240.5/223
Both ^b	BB+PL	2.4(2)	2.1(3)	0.46(5)	220.2/221

^aPL = power law; BB = blackbody

^bEnergy channels between 1.8 and 2.5 keV ignored